

Thiocyanation of *closo*-Dodecaborate $B_{12}H_{12}^{2-}$. A Novel Synthetic Route and Theoretical Elucidation of the Reaction Mechanism

Martin Lepšík,[§] Martin Srnc, [§] Jaromír Plešek,^{†,‡} Miloš Buděšínský,[§] Blanka Klepetářová,[§] Drahomír Hnyk,[‡] Bohumír Grüner,^{*,‡} and Lubomír Rulíšek^{*,§}

[§]*Institute of Organic Chemistry and Biochemistry of the Academy of Sciences of the Czech Republic, Gilead Sciences Research Center, Flemingovo náměstí 2, 166 10 Prague 6, Czech Republic, and*

[‡]*Institute of Inorganic Chemistry of the ASCR, v.v.i., No. 1001, 250 68 Husinec-Řež, Czech Republic*

Received February 2, 2010

Although vast experimental experience has been accumulated about the reactions of icosahedral $B_{12}H_{12}^{2-}$ borane cages, little is known about the mechanisms by which these reactions proceed. To address this issue, we have chosen the thiocyanation of $B_{12}H_{12}^{2-}$ and have studied this reaction using both experimental and theoretical methods. First, we present a novel and more convenient synthetic route using *in situ* generated thiocyanogen, $(SCN)_2$. The synthesized disubstituted product $B_{12}H_{10}(SCN)_2^{2-}$ is exclusively the *meta* positional isomer, as confirmed by the X-ray crystallographic analysis. The quantum chemical calculations at the B3LYP/def2-TZVP//RI-PBE/def2-SVP level show that the free energy differences between the *ortho*, *meta*, and *para* disubstituted species are very small and as such cannot explain the observed positional preferences. The calculations of the kinetic aspects reveal that the reaction is best described as an electrophilic substitution. The calculated isomer preferences for the second SCN substituent are *meta* > *para* > *ortho*. The major outcome of this work is a clear and consistent picture of the electrophilic substitution reaction mechanism of the thiocyanation of $B_{12}H_{12}^{2-}$, thus contributing to our understanding of the general features of boron hydride reactivity.

1. Introduction

The *closo*-dodecaborate dianion ($B_{12}H_{12}^{2-}$, Figure 1a) forms a regular icosahedral cage (I_h symmetry) and is one of the most stable and symmetrical three-dimensional skeletons in all of boron hydride chemistry.¹ The remarkable stability of this formally electron-deficient system stems from the delocalized three-center–two-electron (3c2e) bonding in regular triangular boron facets.^{2,3} In analogy with benzene π -electron delocalization, this σ -bond delocalization has been labeled three-dimensional aromaticity.^{4,5}

A wide spectrum of exosubstitution reactions of $B_{12}H_{12}^{2-}$ has been described. One or more terminal hydrogen atoms can be replaced by, for example, halogens, carbon (leading to various functional groups such as carbonyls and carboxyls),

nitrogen (amines, azides), oxygen (hydroxy), or sulfur (mercapto, thiocyanate) (reviewed in ref 6). In analogy with benzene, positional isomers in the doubly substituted compounds are denoted as *ortho* 1,2- $B_{12}H_{10}X_2^{2-}$ (**2a**), *meta* 1,7- $B_{12}H_{10}X_2^{2-}$ (**2b**), and *para* 1,12- $B_{12}H_{10}X_2^{2-}$ (**2c**, cf. Figure 1). In a few cases, there is experimental evidence for the preferential formation of one positional isomer (e.g., *meta* for halogenations).⁷

Recently, several computational studies have emerged that have dealt with the reaction mechanisms of borane cages.^{8–10} Three examples should be mentioned in brief. For the fluorination of $CB_5H_6^-$ and $CB_9H_{10}^-$, several reaction pathways were explored in terms of the structures of the reaction intermediates along with their energies.⁸ The conclusions were that (i) covalent and ionic pathways had comparable energetic profiles and (ii) substitution at the equatorial boron atom was preferred in agreement with experiment. Another recent study⁹ has proposed three plausible pathways for the

[†] Prof. Jaromír Plešek passed away on April 2, 2010. The authors express their gratitude and remembrance of the work of this outstanding chemist, tutor, and friend and founder of the Czech boron community.

*To whom correspondence should be addressed. Tel: +420-220-183-263. Fax: +420-220-183-578. E-mail: gruner@iic.cas.cz (B.G.); lubos@uochb.cas.cz (L.R.).

(1) Schleyer, P. V.; Najafian, K.; Mebel, A. M. *Inorg. Chem.* **1998**, *37*, 6765–6772.

(2) Lipscomb, W. N. In *Boron Hydrides*; W. A. Benjamin, Inc.: New York, 1963.

(3) Williams, R. E. *Chem. Rev.* **1992**, *92*, 177–207.

(4) King, R. B. *Chem. Rev.* **2001**, *101*, 1119–1152.

(5) Chen, Z. F.; King, R. B. *Chem. Rev.* **2005**, *105*, 3613–3642.

(6) Sivaev, I. B.; Bregadze, V. I.; Sjöberg, S. *Collect. Czech. Chem. Commun.* **2002**, *67*, 679–727.

(7) Lepšík, M.; Srnc, M.; Hnyk, D.; Grüner, B.; Plešek, J.; Havlas, Z.; Rulíšek, L. *Collect. Czech. Chem. Commun.* **2009**, *74*, 1–27.

(8) McKee, M. L. *Inorg. Chem.* **2001**, *40*, 5612–5619.

(9) Rempala, P.; Michl, J. *Collect. Czech. Chem. Commun.* **2003**, *68*, 644–662.

(10) Yoon, C. W.; Kusari, U.; Sneddon, L. G. *Inorg. Chem.* **2008**, *47*, 9216–9227.

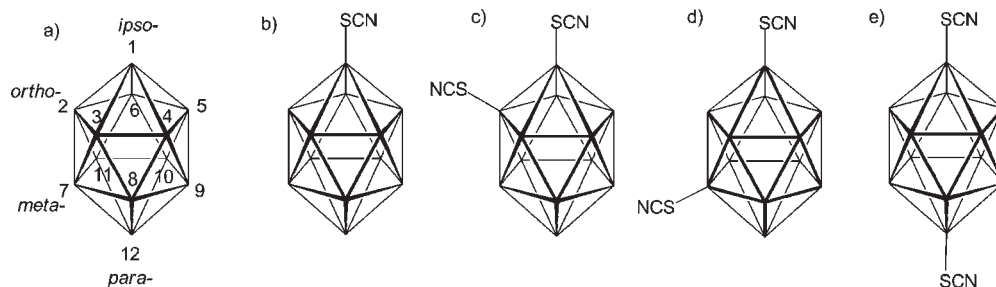


Figure 1. Schematic structures and boron atom numbering of cage boranes discussed in the text. Each vertex stands for a BH group: (a) the icosahedral $B_{12}H_{12}^{2-}$ skeleton; the first exosubstitution occurs at the *ipso* (1) boron vertex, while further modifications can appear in the *ortho* (2–6), *meta* (7–11), or *para* (12) positions; (b) the monosubstituted $B_{12}H_{11}SCN^{2-}$ molecule (**1**); (c, d, and e) the *ortho*-, *meta*- and *para*-disubstituted $B_{12}H_{10}(SCN)_2^{2-}$ (**2a**, **2b**, and **2c**). The atoms of the SCN groups are numbered so as to correspond with the boron vertex to which they are bound (e.g., S1, C1, N1 and S7, C7, N7 for **2b**).

reaction of a dichlorocarbene insertion into *nido*- $B_{11}H_{14}^-$ to yield *closo*- $CB_{11}H_{12}^-$. Quantum mechanical studies¹⁰ have also been performed on alkyne insertion and the olefin hydroboration reactions of $B_{10}H_{13}^-$. Linking the results to their previous experiments, the authors were able to propose a reaction mechanism showing that decaborane can act as either a nucleophile or electrophile, depending on the reaction conditions. Overall, given the vast experimental work done on borane reactions and only a limited number of theoretical studies, we feel a need to provide further mechanistic details to facilitate the understanding of borane reactions.

In our first attempt toward this aim, we investigated the halogenation ($X = F, Cl, \text{ and } Br$) reactions of $B_{12}H_{12}^{2-}$ by experimental as well as computational methods.⁷ The synthesis of the halogenated $B_{12}H_{12}^{2-}$ species proceeded to yield mono-, di-, and trisubstituted species. The disubstituted $B_{12}H_{10}X_2^{2-}$ products contained mostly *meta*- and a small amount of *ortho*-isomer in a ratio of approximately 4:1, whereas no *para*-disubstituted species were detected. In order to rationalize this finding, calculations of the thermodynamic stabilities of all of the potential positional isomers were conducted. The *meta*-disubstituted isomer was found to be the most stable for all of the studied halogens, whereas the *ortho*-isomers were found to be marginally less stable (by 0.6–1.1 kcal·mol⁻¹) at the DFT level.⁷ This result was in very good accord with the experimentally observed *ortho/meta* ratios. However, the stabilities of the *para*-disubstituted products were calculated to be between those of the *meta*- and *ortho*-isomer, in disagreement with experiment. The possible reaction mechanisms were therefore investigated by exploring various pathways for the halogenation reactions of $B_{12}H_{12}^{2-}$, including the structural and energetic characterization of various transition states and reaction intermediates. We were thus able to compare the energetics of several reaction pathways and interpret some of the experimental findings (e.g., chlorination proceeded faster than bromination, the activation barrier for the formation of the *ortho*-isomer was higher than that for the *meta*-isomer), with some discrepancies however remaining (e.g., the reaction barrier for the formation of the *para*-isomer was not prohibitively high, as would have been suggested by the experiments).⁷

In this work, we have focused our efforts on understanding the origin of regioselectivity of the disubstitution reactions of $B_{12}H_{12}^{2-}$ upon thiocyanation. The first procedure, which successfully introduced the SCN functional group into the

$B_{12}H_{12}^{2-}$ boron hydride cluster, made use of thiocyanogen, $(SCN)_2$, in a dichloromethane solution.¹¹ The isolated **1** (Figure 1b) was characterized in terms of its ¹¹B NMR chemical shifts and the IR and Raman spectra. The X-ray crystallographic structure of its cesium salt was determined later.¹² An alternative synthetic route consisted in the application of electrochemical or chemical oxidation (by H_2O_2 or $K_2Cr_2O_7$), yielding both mono- and disubstituted products, the latter as major *meta*- and minor *para*- isomers with no evidence of *ortho*-isomer (Figure 1).¹³

Here, we have described a new preparative method for the synthesis of **1** and **2**, featuring several advantages: this procedure is based on a convenient *in situ* generation of thiocyanogen in the reaction mixture; the product isolation is easier; and the yields are higher than in the above-mentioned approaches of Srebny and Preetz¹¹ and Morris et al.¹³ The reaction products have been characterized using ¹¹B NMR, X-ray crystallography, and quantum chemical calculations of their thermodynamic stabilities. Furthermore, the kinetic aspects of the thiocyanation reaction have been addressed by calculating the activation barriers and characterizing the transition states along the reaction pathway. A plausible mechanism of the thiocyanation reaction of $B_{12}H_{12}^{2-}$ has emerged, reminiscent of electrophilic aromatic substitution in organic chemistry. For the second substitution step, the calculated barriers toward the formation of the three positional isomers (**2a–c**) offer an explanation of the regioselectivity of the disubstitution reaction in accord with experiment. Overall, the presented mechanistic view of the thiocyanation of $B_{12}H_{12}^{2-}$ species extends the general knowledge of reaction mechanisms in boron hydride chemistry.

2. Materials and Methods

Synthesis. The stoichiometries of the thiocyanation reactions of $B_{12}H_{12}^{2-}$ can be described by eqs 3, 4, and 5 (see Results). A detailed description follows.

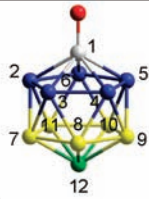
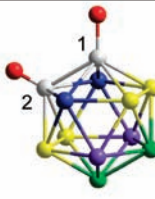
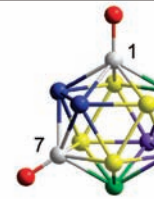
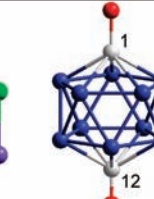
(Et_3NH)₂[$B_{12}H_{11}SCN$] (1**).** A suspension was made from $(Et_3NH)_2B_{12}H_{12}$ (6.92 g, 20.0 mmol) in water (30 mL). This was treated with NaOH (1.6 g, 40.0 mmol) in H_2O (20 mL), and triethylamine was removed under vacuum at 50 °C together with part of the water. The solution of $Na_2B_{12}H_{12}$ in water was then filtered, the pH of the solution was adjusted to 7.0 by a few drops of diluted HCl (1 M, pH metric titration), and the volume was

(12) Sivaev, I. B.; Katser, S. B.; Solntsev, K. A.; Kuznetsov, N. T. *Zh. Neorg. Khim.* **1995**, *40*, 807–810.

(13) Morris, J. H.; Brattsev, V. A.; Gaines, D. F. In *Advances in Boron Chemistry*; Siebert, W., Ed.; RSC: Cambridge, 1997; pp 434–437.

(11) Srebny, H. G.; Preetz, W. Z. *Anorg. Allg. Chem.* **1984**, *513*, 7–14.

Table 1. Mono- and Disubstituted $B_{12}H_{12}^{2-}$ Molecules with Identical Substituents: Their Symmetry Equivalent Positions and the Characteristics of Their ^{11}B NMR Spectra

Type	monosubstituted	disubstituted (identical substituents)		
Isomers		<i>ortho</i> -	<i>meta</i> -	<i>para</i> -
Structures and numbering (substituents shown as red spheres)				
Number of groups of equivalent ^{11}B	4	5	5	2
Point group ^a	C_{5v}	C_{2v}	C_{2v}	D_{5d}
Relative intensities	1 : 5 : 5 : 1	2 : 2 : 4 : 2 : 2	2 : 2 : 4 : 2 : 2	2 : 10
Groups of equivalent ^{11}B signals	white blue yellow green violet	B1 B2–B6 B7–B11 B12	B1, B2 B3, B6 B4, B5, B7, B11 B9, B12 B8, B10	B1, B7 B2, B3 B4, B6, B8, B11 B5, B12 B9, B10
Number of ^{11}B , ^{11}B -COSY cross-peaks of the substituted ^{11}B atom	1	2	3	1

^a In case of equivalent nonlinear substituents the corresponding symmetries are reduced (e.g., from D_{5d} to C_2), and this fact is reflected in the computed spectra (number of peaks increases). However, due to the time scale of the experimental NMR spectroscopy, the number of measured $\delta(^{11}B)$'s is the same as if the substituents were monatomic or linear.

Table 2. Experimental and Calculated ^{11}B Chemical Shifts of $B_{12}H_{11}SCN^{2-}$ (**1**)

method	B1	B2–B6	B7–B11	B12
exptl ^a this work; 160 MHz; CD_3COCD_3 ; $T = +25^\circ C$	−9.0	−13.9	−14.6	−16.6
ref 13	−9.7	−14.4	−14.9	−16.8
ref 11	−9.4		−14.4	−16.5
calcd ^b GIAO-MP2/def2-TZVP	−9.4	−14.4	−15.3	−17.8

^a For additional ^{11}B NMR data see the Supporting Information.
^b Listed values are averages of the individual ^{11}B chemical shifts for equivalent boron atoms according to Table 1 assuming C_{5v} of **1**.

adjusted to 40 mL by water. An aqueous solution of NaSCN (8.92 g, 110 mmol in 15 mL of water) was added, and the solution was heated to 65 °C (bath temperature) and stirred under a nitrogen atmosphere. Subsequently, $CuCl_2 \cdot 2H_2O$ (8.53 g, 50 mmol dissolved in 20 mL of H_2O) was dropwise added during 15 min, and the stirring continued for an additional 30 min, during which the color of the reaction mixture turned shortly to brown, followed by the formation of a white precipitate of $Cu_2(SCN)_2$. Having cooled to room temperature, the precipitate was filtered and washed with water, after which the volume of the filtrate was adjusted to 100 mL, and this solution was heated to the boiling point. An excess of a hot aqueous solution of $Et_3N \cdot HCl$ was subsequently added. After cooling slowly overnight, the solids were collected by filtration and washed with water (2×10 mL). The crude product was treated with hot aqueous ethanol (100 mL), and the hot solution was filtered until it became hot and then was left to crystallize overnight. A white polycrystalline solid was collected and dried under vacuum, with a yield of 7.2 g, 89%. Product **1** was identified by ^{11}B NMR corresponding closely to the previously published data¹¹ and MS (for details, see Supporting Information and Table 2).

Table 3. Experimental and Calculated ^{11}B Chemical Shifts of 1,7- $B_{12}H_{10}(SCN)_2^{2-}$ (**2b**)

method	B1,7	B2,3	B4,6,8,11	B5,12	B9,10
exptl ^a this work; 160 MHz; CD_3COCD_3 ; $T = +25^\circ C$	−8.4	−12.8	−13.3	−13.9	−15.1
calcd ^b GIAO-MP2/def2-SVP	−10.3	−12.1	−10.7	−11.3	−12.1
GIAO-HF/def2-TZVP	−11.6	−12.4	−13.1	−14.1	−16.1

^a For additional ^{11}B NMR data see the Supporting Information.
^b Listed values are averages of the individual ^{11}B chemical shifts for equivalent boron atoms according to Table 1.

(Me₄N)₂[1,7- $B_{12}H_{10}(SCN)_2]$ (2b**).** A 40 mL amount of an aqueous solution of $Na_2B_{12}H_{12}$ prepared from 6.92 g, 20.0 mmol of $(Et_3NH)_2B_{12}H_{12}$ was treated as above with NaSCN (17.84 g, 220 mmol in 20 mL of water), after which $CuCl_2 \cdot 2H_2O$ (17.06 g, 100 mmol, in 25 mL of water) was dropwise added during 15 min at 80 °C, and the reaction mixture was heated under stirring for 2 h. The isolation was performed analogously to the procedure described above, but a solution of Me_4NCl was used to precipitate the crude product. Recrystallization from hot water gave white polycrystalline solids, with a yield of 6.9 g, 85%. The crystal for the X-ray diffraction was grown by a slow cooling of the hot aqueous solution of the salt. The product was identified by ^{11}B NMR corresponding closely to the previously published data¹³ and MS (for details, see Supporting Information and Table 3)

NMR Spectroscopy. Compounds **1**, **2a**, **2b**, and **2c** can be distinguished in the ^{11}B NMR spectra on the basis of their symmetry, which leads to the different number and types of equivalent boron atoms in the molecule, as shown in Table 1. The *ortho*- and *meta*-disubstituted isomers (with identical substituents) have the same number of equivalent boron atoms and relative intensities, but they can be distinguished by the number of cross-peaks of the substituted boron atoms observed in the

$2D\text{-}^{11}\text{B}$, ^{11}B -COSY spectra (two cross-peaks in the *ortho*- and three cross-peaks in the *meta*-disubstituted compound).

Mass Spectrometry. Mass spectrometry measurements were performed on a Thermo-Finnigan LCQ-Fleet ion trap instrument using electrospray (ESI) ionization. Negative ions were detected. Samples, dissolved in acetonitrile (with concentrations of approximately $100\text{ ng}\cdot\text{mL}^{-1}$), were introduced to the ion source by an infusion of $0.25\text{ mL}\cdot\text{h}^{-1}$, a source voltage of 6.0 kV , a tube lens voltage of -54.8 V , a capillary voltage of 10.0 V , a drying temperature of $180\text{ }^\circ\text{C}$, a drying gas flow of 10 L min^{-1} , and an auxiliary gas pressure of 6 bar . Negative ions corresponding to the molecular ion M^{2-} and $[\text{M} + \text{X}]^-$ (where X stands for an alkylammonium cation) were observed. Full agreement of the experimental and calculated isotopic distribution pattern was obtained for both of these peaks. The isotopic distribution in the boron plot of the M^{2-} peaks is in agreement with the charge, showing distances of $1/2$ of the mass units for dianionic compounds. The data are presented for the most abundant mass in the boron distribution plot (100%) and for the peak corresponding to the m/z value.

X-ray Diffraction. An X-ray crystallographic analysis of single crystals of **2b** ($0.03 \times 0.14 \times 0.27\text{ mm}$) was performed using the Xcalibur X-ray diffractometer with $\text{Cu K}\alpha$ ($\lambda = 1.54180\text{ \AA}$), and the data were collected at 150 K . The structure was solved by direct methods with the SIR92 program¹⁴ and refined by full-matrix least-squares methods based on F with the CRYSTALS program.¹⁵ Non-hydrogen atoms were refined with anisotropic thermal displacement parameters; the hydrogen atoms were treated as riding atoms.

Crystal Data. $(\text{Me}_4\text{N})_2[1,7\text{-B}_{12}\text{H}_{10}(\text{SCN})_2]$ (**2b**): monoclinic, space group $P2_1/c$, $a = 10.7534(10)\text{ \AA}$, $b = 19.0294(15)\text{ \AA}$, $c = 12.3953(14)\text{ \AA}$, $\beta = 94.34(4)^\circ$, $V = 2438.0(4)\text{ \AA}^3$, $Z = 4$, $M = 404.27$, 49277 reflections measured, 5062 independent reflections. Final $R = 0.099$, $wR = 0.1095$, $\text{GoF} = 1.125$ for 2409 reflections with $I > 2\sigma(I)$ and 289 parameters. One of the two tetramethylammonium cations was found to be disordered in two positions with their site occupation factors being 0.50 and 0.50. Several restraints were used to regularize its geometry. CCDC 761187 contains the supplementary crystallographic data for this paper including the coordinates. These data can be obtained free of charge from the Cambridge Crystallographic Data Centre via <http://www.ccdc.cam.ac.uk/cgi-bin/catreq.cgi>.

Computational Details. The density functional theory (DFT) calculations reported in the study were carried out using Turbomole 6.0.¹⁶ The Perdew–Burke–Ernzerhof (PBE)¹⁷ and hybrid three-parameter Becke's (B3LYP)¹⁸ functionals were used throughout. For PBE, the calculations were expedited by expanding the Coulomb integrals in an auxiliary basis set, the so-called resolution-of-the-identity (RI-J) approximation in Turbomole.¹⁹ All of the geometry optimizations were carried out without any symmetry constraints using the PBE functional and the def2-SVP basis set.²⁰ The single-point energies were recomputed at the B3LYP level using a larger basis set, def2-TZVP.²⁰

The solvation effects were taken into account by using the Conductor-like Screening Model (COSMO) method²¹ at the RI-PBE/def2-SVP level with a dielectric constant of $\epsilon_r = 80$ for water. As the standard option, we used the Bondi atomic radii multiplied by 1.17. The total Gibbs energy of a molecule was calculated as the sum of the following contributions (eq 1):

$$G = E_{\text{el}} + G_{\text{solv}} + E_{\text{ZPE}} - RT \ln(q_{\text{trans}}q_{\text{rot}}q_{\text{vib}}) \quad (1)$$

where E_{el} is the gas-phase energy of the system (at the B3LYP/def2-TZVP level with the geometry optimized at the RI-PBE/def2-SVP level), G_{solv} is the solvation free energy, E_{ZPE} is the zero-point energy, and $-RT \ln(q_{\text{trans}}q_{\text{rot}}q_{\text{vib}})$ accounts for the entropic terms and for the thermal correction to the enthalpy obtained from a calculation of the analytical harmonic vibrational frequencies at the RI-PBE/def2-SVP level at 298 K and 1 atm , using the ideal-gas approximation.²²

The NMR shieldings (σ_{calc}) of compounds **1** and **2** (designated as X in eq 2) were calculated using the gauge-including atomic orbital many-body second-order perturbation (GIAO-MBPT-(2)) method²³ implemented in the Turbomole package. Two levels of theory employing the coupled perturbed Hartree–Fock (CPHF)²⁴ or Møller–Plesset (MP2) method were used. Two basis sets, namely, def2-SVP and def2-TZVP (for details, see above), were combined with either of the previous two methods. The ^{11}B chemical shifts, $\delta(^{11}\text{B})$, were calculated relative to diborane (B_2H_6) and converted to the standard $\text{BF}_3\cdot\text{OEt}_2$ scale by using an experimental $\delta(^{11}\text{B})$ value of diborane of 16.6 ppm^{25} (eq 2). The $\sigma_{\text{calc}}(\text{diborane})$ values computed at the HF/def2-SVP, MP2/def2-SVP, HF/def2-TZVP, and MP2/def2-TZVP levels were 106.8, 104.4, 100.3, and 95.8 ppm, respectively:

$$\delta(^{11}\text{B})_{\text{X}} = \delta(^{11}\text{B})_{\text{B}_2\text{H}_6} + \sigma_{\text{calc}}(\text{B}_2\text{H}_6) - \sigma_{\text{calc}}(\text{X}) \quad (2)$$

The thermodynamic stabilities of **2a–c** were calculated in two steps. First, the potential energy surfaces of various relative rotational conformers (rotamers) of both of the SCN groups were evaluated at the RI-PBE/def2-SVP level using two-dimensional relaxed potential energy scans of the two C–S–B–B dihedrals (for details, see Supporting Information). Second, several low-energy conformers were reoptimized without any constraints at the RI-PBE/def2-SVP level. The total Gibbs energy was calculated according to eq 1.

The geometries of $\text{B}_{12}\text{H}_{12}^{2-}$, **1**, and **2** were taken from the relevant crystal structures (CSD code FUYZOO²⁶ for $\text{B}_{12}\text{H}_{12}^{2-}$, ZASYEX¹² for **1**, or this work for **2b**), while **2a** and **2c** geometries were built by analogy. The structure of $(\text{SCN})_2$ was built according to ref 27.

The transition states of the reactions were searched starting from estimates obtained from relaxed potential energy scans of the incipient B–S distance (in the $2.0\text{--}3.2\text{ \AA}$ range at 0.2 \AA steps), the S–S distance in thiocyanogen (in the $2.2\text{--}3.2\text{ \AA}$ range at 0.2 \AA steps), and the B–S–S angle (from 50° to 170°). These estimates were further refined by diagonalization of the Hessian matrix using the AOFORCE module in Turbomole 6.0 and by optimizations along the selected transition vectors. The relevancy of the located transition state was confirmed by the

(14) Altomare, A.; Cascarano, G.; Giacovazzo, G.; Guagliardi, A.; Burla, M. C.; Polidori, G.; Camalli, M. *J. Appl. Crystallogr.* **1994**, *27*, 435–436.

(15) Betteridge, P. W.; Carruthers, J. R.; Cooper, R. I.; Prout, K.; Watkin, D. J. *J. Appl. Crystallogr.* **2003**, *36*, 1487–1487.

(16) Ahlrichs, R.; Bär, M.; Häser, M.; Horn, H.; Kölmel, C. *Chem. Phys. Lett.* **1989**, *162*, 165–169.

(17) Perdew, J. P.; Burke, K.; Ernzerhof, M. *Phys. Rev. Lett.* **1996**, *77*, 3865–3868.

(18) (a) Becke, A. D. *Phys. Rev. A* **1988**, *38*, 3098–3100. (b) Lee, C. T.; Yang, W. T.; Parr, R. G. *Phys. Rev. B* **1988**, *37*, 785–789. (c) Becke, A. D. *J. Chem. Phys.* **1993**, *98*, 5648–5652. (d) Stephens, P. J.; Devlin, F. J.; Chabalowski, C. F.; Frisch, M. J. *J. Phys. Chem.* **1994**, *98*, 11623–11627.

(19) (a) Eichkorn, K.; Treutler, O.; Ohm, H.; Häser, M.; Ahlrichs, R. *Chem. Phys. Lett.* **1995**, *240*, 283–290. (b) Eichkorn, K.; Weigen, F.; Treutler, O.; Ahlrichs, R. *Theor. Chim. Acta* **1997**, *97*, 119–124.

(20) Weigend, F.; Ahlrichs, R. *Phys. Chem. Chem. Phys.* **2005**, *7*, 3297–3305.

(21) (a) Klamt, A.; Schuurmann, G. *J. Chem. Soc., Perkin Trans. 2* **1993**, 799–805. (b) Schäfer, A.; Klamt, A.; Sattler, D.; Lohrenz, J. C. W.; Eckert, F. *Phys. Chem. Phys.* **2000**, *2*, 2187–2193.

(22) Jensen, F. In *Introduction to Computational Chemistry*; John Wiley & Sons: New York, 1999.

(23) Kollwits, M.; Gauss, J. *Chem. Phys. Lett.* **1996**, *260*, 639–646.

(24) Ziegler, T.; Schreckenbach, G. *J. Phys. Chem.* **1995**, *99*, 606–611.

(25) Onak, T. P.; Landesman, H. L.; Williams, R. E.; Shapiro, I. J. *Phys. Chem.* **1959**, *63*, 1533–1535.

(26) Wunderlich, J. A.; Lipscomb, W. N. *J. Am. Chem. Soc.* **1960**, *82*, 4427–4428.

(27) Jensen, J. *J. Mol. Struct. (THEOCHEM)* **2005**, *714*, 137–141.

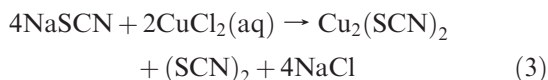
determination of a single imaginary vibrational frequency of a transition vector, which pointed in both the forward and backward directions of the reaction pathway.

The charge analyses, carried out using the Gaussian 03 package,²⁸ were based on the fits to the electrostatic potential (ESP) calculated at the B3LYP/cc-pVTZ level using the Pauling radii in an implicit IEFPCM solvent model²⁹ with a dielectric of $\epsilon_r = 4$. The choice of atomic radii differs from that used for treating solvation effects (COSMO model) above to conform to the original parametrization of the ESP analysis.

3. Results

3.1. Synthesis of 1 and 2. An alternative synthetic route leading to the mono- and dithiocyanate derivatives of $B_{12}H_{12}^{2-}$ ion is presented. The approach is based on an oxidative generation of thiocyanogen $(SCN)_2$ *in situ* in the reaction mixture by heating sodium thiocyanate and copper(II) dichloride in water (eq 3). The thiocyanogen itself is unstable, may be subjected to several decomposition pathways, and should rather be thought of as an equilibrium mixture.³⁰ An important route is a rapid decomposition of $(SCN)_2$ in water to polymerize irreversibly to a brick-red polythiocyanogen. No such coloration is observed during the reactions. It indicates that the *in situ* formed thiocyanogen reacts preferentially and quantitatively with $B_{12}H_{12}^{2-}$ up to disubstitution.

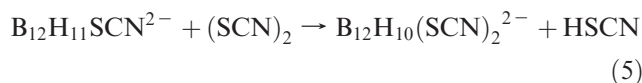
The reaction of $(SCN)_2$ with $B_{12}H_{12}^{2-}$ can be described as a notional metathesis in which one hydrogen atom of $B_{12}H_{12}^{2-}$ is exchanged for an SCN group, thus forming **1** and HSCN (eq 4). The substitution of another hydrogen atom of $B_{12}H_{12}^{2-}$ with another SCN group leads to **2b** (eq 5). These reactions are exceptionally clean, giving high yields of both **1b** and **2b** (89% and 85%, respectively) after simple isolation steps. Regioselective disubstitution (eq 5) of the boron cage leading to only the **2b** isomer was observed, with no sign of the presence of other possible isomers (**2a** or **2c**). The products **1** and **2b** have been characterized by the NMR and MS data, along with a full report on the solution of the $(Me_4N)_2[1,7-B_{12}H_{10}(SCN)_2]^{2-}$ structure by X-ray diffraction and the complete set of the structural data (see below).



(28) Frisch, M. J.; Trucks, G. W.; Schlegel, H. B.; Scuseria, G. E.; Robb, M. A.; Cheeseman, J. R.; Montgomery, J. A., Jr.; Vreven, T.; Kudin, K. N.; Burant, J. C.; Millam, J. M.; Iyengar, S. S.; Tomasi, J.; Barone, V.; Mennucci, B.; Cossi, M.; Scalmani, G.; Rega, N.; Petersson, G. A.; Nakatsuji, H.; Hada, M.; Ehara, M.; Toyota, K.; Fukuda, R.; Hasegawa, J.; Ishida, M.; Nakajima, T.; Honda, Y.; Kitao, O.; Nakai, H.; Klene, M.; Li, X.; Knox, J. E.; Hratchian, H. P.; Cross, J. B.; Bakken, V.; Adamo, C.; Jaramillo, J.; Gomperts, R.; Stratmann, R. E.; Yazyev, O.; Austin, A. J.; Cammi, R.; Pomelli, C.; Ochterski, J. W.; Ayala, P. Y.; Morokuma, K.; Voth, G. A.; Salvador, P.; Dannenberg, J. J.; Zakrzewski, V. G.; Dapprich, S.; Daniels, A. D.; Strain, M. C.; Farkas, O.; Malick, D. K.; Rabuck, A. D.; Raghavachari, K.; Foresman, J. B.; Ortiz, J. V.; Cui, Q.; Baboul, A. G.; Clifford, S.; Cioslowski, J.; Stefanov, B. B.; Liu, G.; Liashenko, A.; Piskorz, P.; Komaromi, I.; Martin, R. L.; Fox, D. J.; Keith, T.; Al-Laham, M. A.; Peng, C. Y.; Nanayakkara, A.; Challacombe, M.; Gill, P. M. W.; Johnson, B.; Chen, W.; Wong, M. W.; Gonzalez, C.; Pople, J. A. *Gaussian 03, revision C.02*; Gaussian, Inc.: Pittsburgh, PA, 2003.

(29) (a) Cancès, M. T.; Mennucci, B.; Tomasi, J. *J. Chem. Phys.* **1997**, *107*, 3032–3041. (b) Mennucci, B.; Tomasi, J. *J. Chem. Phys.* **1997**, *106*, 5151–5158.

(30) Barnett, J. J.; McKee, M. L.; Stanbury, D. M. *Inorg. Chem.* **2004**, *43*, 5021–5033.



3.2. Structural and NMR Characterization of 1 and 2b.

The 3D structure of **1** as a Cs^+ salt has been determined previously by X-ray crystallography (CSD code: ZASYEX).¹² The noteworthy feature is that the linear SCN group was bound to the *ipso*-boron vertex at an obtuse C1–S1–B1 angle of 102°. The two Cs^+ counterions are located above the BBB triangles and interact with the hydrogen atoms of the cage via six interactions with distances ranging from 2.9 to 3.4 Å.

In order to have a consistent set of data with **2b** (*vide infra*), the ^{11}B NMR spectra were measured. The chemical shifts are reported in Table 2, along with the previously published data. All of the data clearly show a trend of increasing downfield chemical shifts with increasing distance from the *ipso*-boron vertex. It can be noted that various approaches yield results that differ by at most 0.7 ppm.

As a theoretical complement, the ^{11}B NMR chemical shifts of **1** were computed for the optimized (equilibrium) geometries using the GIAO approach at the two levels of theory, the Hartree–Fock and MP2, and two basis sets, def2-SVP and def2-TZVP. The full set of data is available in the Supporting Information (Table S2), whereas the most accurate MP2/def2-TZVP values are shown in Table 2. The experimentally observed trends are reproduced by all of the methods. In the case of the GIAO-MP2/def2-TZVP method, the largest deviation from the experiment is 1.3 ppm (Table 2).

1,7- $B_{12}H_{10}(SCN)_2^{2-}$. The three-dimensional structure of $(Me_4N)_2[1,7-B_{12}H_{10}(SCN)_2]$ was determined by X-ray diffraction (Figure 2). The two SCN groups were bound to the $B_{12}H_{12}^{2-}$ cage with C1–S1–B1–B2 and C7–S7–B7–B3 dihedral angles of -113° and 34° , respectively. The two tetramethylammonium cations interacted with the cage via a total of four C–H···H–B dihydrogen bonds with H–H distances ranging from 2.3 to 2.8 Å.

The ^{11}B NMR spectra were measured for **2b** and calculated at the optimized geometry corresponding to the isomer obtained by X-ray diffraction (Table 3). The best theoretical approach, MP2/def2-TZVP, used for **1** is beyond the computational possibilities for **2b**, and thus the results of two inferior methods, namely, MP2/def2-SVP and HF/def2-TZVP, have been shown. Consistent with our previous finding,⁷ the latter method is in better agreement with experiment. It reproduces the experimentally observed trends and quantitatively yields an agreement to within 1 ppm, except for the B1 and B7 positions, where the difference is 3.2 ppm.

3.3. Positional Preferences of $B_{12}H_{10}(SCN)_2^{2-}$. As described in eq 5, the prolonged reaction time (2 h) of $B_{12}H_{12}^{2-}$ with thiocyanogen yielded disubstituted $B_{12}H_{10}(SCN)_2^{2-}$ but only as its *meta* positional isomer, **2b**. The reason that other positional isomers were not observed is addressed here by calculations of the thermodynamic stabilities of **2a**, **2b**, and **2c**. These energies may be dependent on the relative orientations of the two thiocyanato groups bound to the

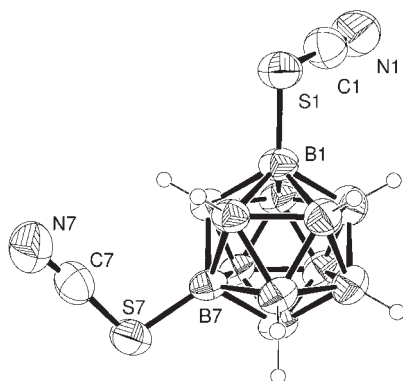


Figure 2. ORTEP representation of the crystallographic structure of **2b**. The thermal ellipsoids are drawn at the 50% probability level. Two counterions are not shown for the sake of clarity.

$B_{12}H_{12}^{2-}$ cage (rotamers), and therefore we undertake a two-step procedure. First, the potential energy surface (PES) corresponding to the various rotamers is described for the *ortho*-, *meta*-, and *para*-isomers. Figure S1 (see Supporting Information) shows that the PESs are quite flat for the *meta*- and *para*-isomers (the energies are within $1 \text{ kcal}\cdot\text{mol}^{-1}$), while for the *ortho*-isomer the energy differences amount to several $\text{kcal}\cdot\text{mol}^{-1}$. This finding is understandable given the spatial closeness of the two SCN groups in the **2a** species and the assumed steric clashes for C1–S1–B1–B2 and C2–S2–B2–B1 dihedrals around the values of -72° and 72° , respectively. The second step consists in reoptimizing several low-energy rotamers (see Table S1 in the Supporting Information) without any constraints and calculating their free energies according to eq 1. The three minima for *ortho*-, *meta*-, and *para*-isomers are characterized by their geometrical parameters (two C–S–B–B dihedrals; see the Supporting Information) and their relative energies: **2a** (-117° ; -114° ; $0.4 \text{ kcal}\cdot\text{mol}^{-1}$), **2b** (172° ; -51° ; $0 \text{ kcal}\cdot\text{mol}^{-1}$), **2c** (-6° ; -35° ; $-0.4 \text{ kcal}\cdot\text{mol}^{-1}$). For comparison, we conducted the same computational procedure for the optimized X-ray structure of **2b** (-113° , 34° ; $0.2 \text{ kcal}\cdot\text{mol}^{-1}$). The tiny free energy difference between the two conformers of **2b**, which differ substantially in their C–S–B–B dihedral angles, suggests that the two SCN ligands bound to the $B_{12}H_{12}^{2-}$ cage can rotate freely.

It can be concluded that (i) the free energy differences in the thermodynamic stabilities of all the disubstituted regioisomers of $B_{12}H_{10}(SCN)_2^{2-}$ (**2a**, **2b**, and **2c**) are very small and well within the error bars of the computational protocol used and (ii) **2a–c** possess a high degree of rotational freedom, which is also reflected in NMR spectroscopy measurements, where an averaging of the signals for equivalent boron atoms occurs. Due to (i), the calculation of thermodynamic stabilities cannot account for the experimentally observed exclusive formation of the 1,7- $B_{12}H_{10}(SCN)_2^{2-}$ isomer. We thus turn our attention to the kinetic aspects of the thiocyanation reaction of $B_{12}H_{12}^{2-}$.

3.4. Reaction Mechanism. Let us consider the first reaction step described by eq 3. This is an endergonic redox reaction (the standard reduction potential E^0 of SCN^0/SCN^- and Cu^{2+}/Cu^+ pairs is 0.77 and 0.16 V vs SHE,

respectively;³¹ i.e., $\Delta G^0_{\text{redox}} = +0.61 \text{ eV}$), which can proceed only at the cost of added energy (heat). In the second reaction step (eq 4), the *in situ* formed thiocyanogen ($SCN)_2$ reacts with the $B_{12}H_{12}^{2-}$ cage (which itself has a large reduction potential of $E^0 = 1.41 \text{ V vs SHE}$) to exchange one of its terminal hydrogens for an SCN group, thus forming **1** and HSCN. Although we cannot completely exclude a radical mechanism, the experimental evidence of the $Cu_2(SCN)_2$ white precipitate indicates that the redox reaction occurs between SCN^0/SCN^- and Cu^{2+}/Cu^+ pairs. Thus, further steps should involve SCN^+/SCN^- species.

Upon encounter of the two reactants, a reactant complex is formed (representing a minimum on the potential energy surface) in which the S1 atom of the thiocyanogen attacks the H-*ipso* hydrogen of $B_{12}H_{12}^{2-}$ (see Figure 3 and the Supporting Information). The electrophilic character of the attacking S1 atom can be inferred either from its partial positive charge of $+0.1e$ or alternatively from the presence of a patch of positive electrostatic potential on the axis of the S–S bond. (The electrophilicity of the entire thiocyanogen molecule is mentioned in the Discussion.) The attacked *ipso* hydrogen of $B_{12}H_{12}^{2-}$ has a partial negative charge of $-0.2e$. An overall charge transfer of $0.3e$ occurs from $B_{12}H_{12}^{2-}$ to $(SCN)_2$. The formation of the complex is favorable in the gas phase (with an energy difference of $-29.2 \text{ kcal}\cdot\text{mol}^{-1}$ at the B3LYP/def2-TZVP level), but the solvation terms ($41.2 \text{ kcal}\cdot\text{mol}^{-1}$) and free energy corrections ($8.0 \text{ kcal}\cdot\text{mol}^{-1}$) reverse the sign to make this complex formation unfavorable. Further progress along the reaction coordinate leads to the transition state (TS) (Figure 3A), which is characterized by (i) the formation of the B1–S1 bond (2.1 \AA) (for atom numbering, see Figure 1), (ii) a weakening of the S1–S2 bond (with the distance increased from 2.1 to 3.1 \AA), (iii) a single imaginary-frequency mode ($221i \text{ cm}^{-1}$) pointing along the reaction coordinate, and (iv) a free energy barrier with respect to the separated reactants of $23.0 \text{ kcal}\cdot\text{mol}^{-1}$. In the transition state, a further charge transfer occurs from $B_{12}H_{12}^{2-}$ to the S2 and N2 atoms of thiocyanogen, so that an SCN^- anion ($-0.9e$) is created.

This nucleophilic moiety attracts the H-*ipso* proton and in the further course of the reaction forms the leaving HSCN molecule (*Hipso*–S2–C2–N2). Thus, **1** is also formed. A complex of the two products with an $SH\cdots S$ type of interaction has a relative free energy of $-18.2 \text{ kcal}\cdot\text{mol}^{-1}$. The separation of the products is predicted to be strongly exergonic (with a relative energy of $-30.9 \text{ kcal}\cdot\text{mol}^{-1}$). We have thus found a plausible reaction mechanism of the formation of **1** and HSCN starting from $B_{12}H_{12}^{2-}$ and thiocyanogen.

The **2a–c** can be formed in an analogous way (Figure 3B). The only minor difference is that the barriers to the transition states are higher by $2.5\text{--}5.0 \text{ kcal}\cdot\text{mol}^{-1}$ than they were for the first thiocyanation reaction. The free energy barriers for the formation of the transition states leading to **2b** and **2c** are similar, differing by only $0.1 \text{ kcal}\cdot\text{mol}^{-1}$, while the TS leading to **2a** is $2.5 \text{ kcal}\cdot\text{mol}^{-1}$ higher in energy (Figure 3B). The formation of **2b** is slightly favored over **2c** due to the 5-fold higher frequency factor. Taken together, the calculated TS barriers along with simple structural reasoning suggest that the order of kinetic preferences for the formation of the positional isomers of the disubstituted $B_{12}H_{10}(SCN)_2^{2-}$ is *meta* > *para* > *ortho*.

(31) Bard, A. J.; Parsons, R.; Jordan, J. *Standard Potentials in Aqueous Solutions*; Marcel Dekker: New York, 1985.

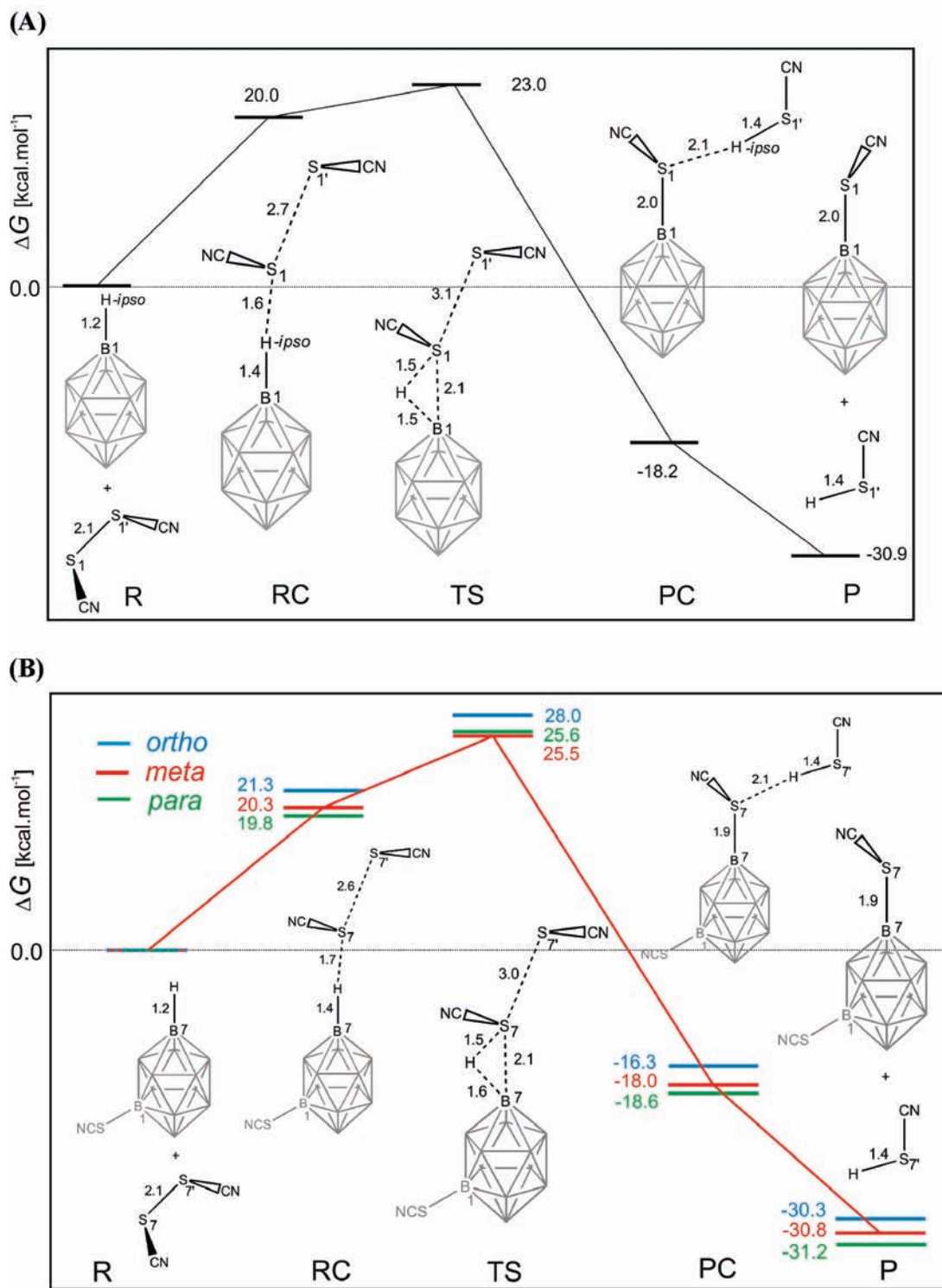


Figure 3. Reaction pathway for the thiocyanation of (A) $B_{12}H_{12}^{2-}$ and (B) $B_{12}H_{11}SCN^{2-}$ (**1**) with $(SCN)_2$. The schematic structures of reactants (R), reactant complexes (RC), transition states (TS), product complexes (PC), and products (P) are shown along with their key geometrical parameters and the calculated relative free energies. In (B), the structures are shown only for the observed **2b** pathway, while the calculated energies are also included for the theoretical *ortho*- and *para*-disubstituted products.

This conclusion is in agreement with the experimentally observed formation of **2b**, while not completely explaining why **2c** was not formed as a minor product (see Discussion).

4. Discussion

4.1. Synthesis of 1 and 2. In this study, we present an alternative and more convenient preparative method for

the synthesis of mono- and dithiocyanato-substituted $B_{12}H_{12}^{2-}$ in aqueous solution employing *in situ* formed thiocyanogen. The previously published approaches either utilized the reaction of $B_{12}H_{12}^{2-}$ with thiocyanogen in dichloromethane¹¹ or used an electrochemical or chemical oxidation of thiocyanate salts.¹³ The disadvantages of these approaches were the intrinsic instability of

thiocyanogen, the solvent used, and the additions of H_2O_2 or $\text{K}_2\text{Cr}_2\text{O}_7$ to $\text{Na}_2\text{B}_{12}\text{H}_{12}$ for the chemical oxidation, which may, under less perfectly controlled conditions and on a larger scale, lead to hydroxylated derivatives or to spontaneous ignition. In contrast, the procedure presented here generates thiocyanogen *in situ* in controlled conditions by heating of CuCl_2 and NaSCN (eq 3). This is an endergonic redox reaction occurring at the expense of added heat where the thiocyanogen is generated in a controlled manner for the subsequent reaction steps (eqs 4, 5) and shifts the equilibrium toward the products. We assume that the thiocyanogen does not behave as a hot species. Due to the polarizability of the divalent sulfur in disulfide compounds, the S–S bond tends to be cleaved by polar reagents, electrophiles, and especially nucleophiles. Finally, this procedure is general and has a broader applicability in heteroborane chemistry.

4.2. ^{11}B NMR and X-ray Crystallographic Data for **1 and **2**.** Our ^{11}B chemical shifts (obtained using the Varian Mercury 400 Plus and Bruker Avance 500 instruments) for compound **1** are in agreement with the previously published values reported by Srebny and Preetz¹¹ and Morris et al.¹³ (cf. Table 2). The previously determined crystal structure of the cesium salt of **1**¹² then served as a starting geometry for the theoretical calculations. Much less information is, however, available for compound **2**. It has been reported that the electrochemical or chemical oxidation of thiocyanate salts yielded mainly **2b**, while the **2c** constituted a minor product.¹³ However, only an incomplete set of NMR and X-ray data for **2b** and **2c** was published.¹³ In comparison, in our synthetic approach an exclusive formation of **2b** in the isolated solid product was observed (using HPLC and mass spectrometry), and this compound was characterized by NMR and X-ray crystallography. It is unclear whether the absence of the *para*-isomer was caused by its inherent kinetic or thermodynamic properties or by different reagents used in this work, which may, for some reason, prevent its appearance. Furthermore, we cannot completely rule out that small quantities of **2c** were present in the mother liquors after crystallization.

4.3. Reaction Mechanism. On the basis of the quantum chemical calculations, we propose a plausible reaction mechanism for the thiocyanation of $\text{B}_{12}\text{H}_{12}^{2-}$. It can be described as electrophilic substitution (S_{E}), which has been put forward before as a possible reaction type in the realm of boron hydride chemistry.³² The two main characteristics of the proposed S_{E} reaction type are the presence of an electrophile and an intermediate state called a σ -complex, in analogy to organic chemistry.³²

The electrophilicity of the reacting $(\text{SCN})_2$ can be manifested using two different approaches. First, it is the partial positive charge of $+0.1e$ on the S1 atom or alternatively the presence of a patch of positive electrostatic potential on the axis of the S–S bond. It should be noted that both the high polarizability of sulfur and the electron-withdrawing capability of the cyano groups make this localized electron deficiency stronger.³³

Second, it is reflected by the ability of its S–S antibonding orbital to accept a charge from the $\text{B}_{\text{ipso}}\text{–H}$ bonding orbital of $\text{B}_{12}\text{H}_{12}^{2-}$, as is suggested by NBO analysis.

The transition state that we obtained is characterized by the newly created B1–S1 bond while still retaining the B1–H-*ipso* bond (Figure 3). In this respect (the simultaneous binding of the original proton and the incoming electrophile by the *ipso* atom), our TS structure is in accord with the σ -complex state proposed for the S_{E} reaction type in borane chemistry.³²

According to our mechanism, the progress of the thiocyanation reaction is made through abstracting the *ipso* proton by a distant nucleophilic SCN^- group (Lewis base), whereas the other SCN group remains attached to the $\text{B}_{12}\text{H}_{12}^{2-}$ cage (in effect, the close SCN group has been exchanged for the *ipso* proton). It was debated whether the rate-limiting step of the S_{E} reactions of boranes was the formation of the σ -complex or rather the ensuing proton transfer process.³² Our calculations clearly show that for the case of the thiocyanation of $\text{B}_{12}\text{H}_{12}^{2-}$ the former hypothesis is true; the transition state formation has a free energy barrier of $23.0 \text{ kcal}\cdot\text{mol}^{-1}$, while the proton transfer process is barrierless and energetically favorable (the product complex has a relative free energy of $-18.2 \text{ kcal}\cdot\text{mol}^{-1}$).

The presented reaction mechanism is analogous to that found in our previous study for the halogenation of $\text{B}_{12}\text{H}_{12}^{2-}$ with X_2 ($\text{X} = \text{Cl}, \text{Br}$).⁷ A brief comparison reveals that the charge distribution in the reactant complex and the TS for halogenations (for eqs 4a and b in the original paper; no charge analysis was reported)⁷ are consistent with the S_{E} mechanism presented here for thiocyanation. The transition state barriers were smaller for halogenations ($\Delta G_{\text{calc}}^\ddagger = 0.1$ and $8.7 \text{ kcal}\cdot\text{mol}^{-1}$ for chlorination and bromination, respectively) than for thiocyanation ($\Delta G_{\text{calc}}^\ddagger = 23.0 \text{ kcal}\cdot\text{mol}^{-1}$). The exergonicity of halogenations was also larger (-55.9 and $-35.9 \text{ kcal}\cdot\text{mol}^{-1}$ for chlorination and bromination, respectively) when compared to thiocyanation ($-30.9 \text{ kcal}\cdot\text{mol}^{-1}$), suggesting the order of reaction rates of $\text{Cl} > \text{Br} > \text{SCN}$. This finding is in accord with experiment, where the chlorination and bromination reactions proceeded faster and to a higher degree of substitution than with thiocyanation.

Although our calculations presented here and in our previous work⁷ give support to the electrophilic substitution mechanism for the thiocyanation and halogenation (using X_2 , $\text{X} = \text{Cl}$ and Br) of $\text{B}_{12}\text{H}_{12}^{2-}$, we should bear in mind that other reactions of heteroboranes may proceed via the postulated electrophile-induced nucleophilic substitution (EINS) mechanism.³² Indeed, the EINS mechanism was described computationally for the fluorination of CB_5H_6^- and $\text{CB}_9\text{H}_{10}^-$ carboranes⁸ and $\text{B}_{12}\text{H}_{12}^{2-}$ using hydrogen fluoride.⁷ The electrophile was H^+ , the leaving group was H_2 , and the nucleophile was F^- . For the two cage carboranes, two pathways, concerted and ionic, were evaluated and found to be comparable in energy.

Finally, the reliability of our computational protocol has to be discussed. In the construction of the total Gibbs energy (see Methods) we apply the thermodynamic cycle, i.e., ΔG is a sum of the ΔG_{vac} (in order for the ideal-gas approximation for the vibrational analysis to be valid) and the ΔG_{solv} , evaluated using the implicit model. Systematic errors are associated with both of these terms

(32) Körbe, S.; Schreiber, P. J.; Michl, J. *Chem. Rev.* **2006**, *106*, 5208–5249.

(33) Murray, J. S.; Lane, P.; Clark, T.; Politzer, P. J. *Mol. Model.* **2007**, *13*, 1033–1038.

as well as due to the thermodynamic cycle decomposition scheme.

The uncertainty in the gas-phase transition state barriers calculated at the B3LYP level is generally not expected to be below 3–5 kcal·mol⁻¹ (ref 34). Second, the use of an implicit solvation model results in deviations from experiment of approximately 4 kcal·mol⁻¹ for ionic molecules.³⁵ Further errors may stem from the lack of explicit treatment of solvent molecules. However, finding their configuration would require a quantum dynamical simulation, which is beyond the scope of this study.

The second group of errors can be observed as a difference in geometries optimized in the gas phase and in solution. In the test calculations these changes were negligible; the largest one was observed in the reactant complex in which the S1–S1' distance was 0.4 Å larger under vacuum than in solution. The comparison of the total Gibbs energies of these two conformers revealed a difference of $\Delta G = 6.3$ kcal·mol⁻¹ in favor of the latter. However, this difference reduced to ~1 kcal·mol⁻¹ in the calculated activation barrier (ΔG^\ddagger) and can serve as an estimate of the error associated with our thermodynamic-cycle decomposition scheme. Despite the quantitative uncertainties, we feel that our computational approach can provide us with a semiquantitative understanding of the reaction mechanism.

4.4. Directive Effects of the SCN Substituent on the B₁₂H₁₂²⁻ Cage. To address this question, we performed a quantum chemical study of the reaction mechanisms of the second thiocyanation of **1**. The calculated order of kinetic preferences for the disubstituted B₁₂H₁₀(SCN)₂²⁻ was *meta* > *para* > *ortho*. The former preference was attributed to a 5:1 ratio of boron vertices available for the attack, as the thermodynamic stability and kinetic accessibility of **2b** and **2c** were predicted to be almost the same (within tenths of kcal·mol⁻¹). However, with such tiny energy differences and the quantitative uncertainties of our computational protocol, we must be cautious not to overinterpret our results. The *meta* > *ortho* preference is then explained by the higher barrier for the *ortho* isomer by 2.5 kcal·mol⁻¹. In terms of acceleration of the reaction, this translates, using the Arrhenius equation, into a 66-fold increase in the reaction rate for **2b** with respect to **2a**, which would preclude an experimental observation of the *ortho*-isomer as the reaction product.

In our previous work⁷ on halogenations of B₁₂H₁₂²⁻, we came to similar conclusions on the *ortho*-disubstituted B₁₂H₁₂²⁻ having a higher barrier of formation than *meta*, with the *para*-isomer being comparable in energy but having a lower frequency factor. Both studies thus showed a kinetic preference of the *meta*-disubstituted

B₁₂H₁₂²⁻, in accord with the experiment. Moreover, the calculations afforded a mechanistic insight into the electrophilic substitution reaction mechanism of boranes.

5. Conclusions

The thiocyanation of the icosahedral B₁₂H₁₂²⁻ borane cage to yield monosubstituted B₁₂H₁₁SCN²⁻ and disubstituted B₁₂H₁₀(SCN)₂²⁻ products was studied both experimentally and computationally. A novel, more convenient synthetic route using *in situ* generated thiocyanogen, (SCN)₂, was presented here. All the products were characterized using mass spectrometry and NMR spectroscopy. The ¹¹B NMR chemical shifts (magnetic shieldings) were calculated at the MP2 level, and close agreement (mostly within 1 ppm) with their experimental counterparts was found. The synthesized disubstituted product was found to be exclusively the *meta* positional isomer, confirmed by the X-ray crystal structure. Quantum chemical calculations were undertaken to evaluate the positional preferences of the second SCN substituent on B₁₂H₁₂²⁻ and to study the mechanism of the thiocyanation reactions. In terms of thermodynamic stabilities, only slight differences between *ortho*-, *meta*-, and *para*-disubstituted species were found. The calculations revealed that the reaction is best described as an electrophilic substitution with a barrier of 23.0 kcal·mol⁻¹ and exergonicity of -30.9 kcal·mol⁻¹. The transition states corresponding to the formation of the disubstituted products had similar free energy for the *meta*- and *para*-isomers, while for the *ortho* the TS was 2.5 kcal·mol⁻¹ higher. The frequency factor ratio of 5:1 for substitutions at the *meta* and *para* vertices, respectively, favors the former, while not completely excluding the latter. Taken together, our calculations predict the order of preference of the formation to be *meta* > *para* > *ortho*. In summary, we feel that the major outcome of this work is a clear and consistent picture of the electrophilic substitution reaction mechanism of the thiocyanation of B₁₂H₁₂²⁻, thus contributing to our understanding of the general features of boron hydride reactivity. We believe that such a mechanistic understanding of cage borane reactions is essential for further predictions of the reactive patterns of other boranes and heteroboranes.

Acknowledgment. The financial support of the Ministry of Education of the Czech Republic (LC523, LC512), ASCR (AV0Z40320502 and Z40550506), and the Grant Agency of the Academy of Sciences of the Czech Republic (IAAX00320901) is gratefully acknowledged. We also thank Dr. Jindřich Fanfrlík for his help with the charge analysis and Dr. Miller for language corrections.

Supporting Information Available: The geometries of all the transition states, the potential energy surfaces of dihedral scans of the thiocyanate groups of **2a**, **2b**, and **2c**, as well as the MS data of **1** and **2b** and ¹¹B NMR chemical shifts of **1** and **2** calculated at several levels of theory are available free of charge via the Internet at <http://pubs.acs.org>.

(34) Harvey, J. N. *Faraday Discuss.* **2009**, *145*, 487–505.

(35) (a) Marenich, A. V.; Cramer, C. J.; Truhlar, D. G. *J. Phys. Chem. B* **2009**, *113*, 6378–6396. (b) Kongsted, J.; Söderhjelm, P.; Ryde, U. *J. Comput.-Aided Mol. Des.* **2009**, *23*, 395–409.